Biology of Cancer and PET Imaging: Pictorial Review

Ismet Sarikaya

Kuwait University Faculty of Medicine and Mubarak Al-Kabeer Hospital Department of Nuclear Medicine, Kuwait City, Kuwait

CE credit: For CE credit, you can access the test for this article, as well as additional *JNMT* CE tests, online at https://www.snmmilearningcenter.org. Complete the test online no later than June 2025. Your online test will be scored immediately. You may make 3 attempts to pass the test and must answer 75% of the questions correctly to receive Continuing Education Hour (CEH) credit. Credit amounts can be found in the SNMMI Learning Center Activity. SNMMI members will have their CEH credit added to their VOICE transcript automatically; nonmembers will be able to print out a CE certificate upon successfully completing the test. The online test is free to SNMMI members; nonmembers must pay $15.00 by credit card when logging onto the website to take the test.

Development and spread of cancer is a multistep and complex process that involves a number of alterations, interactions, and molecular networks. PET imaging is closely related to cancer biology and pathology, as it uses various radiotracers targeting biologic and pathologic changes in cancer cells and the tumor microenvironment. In this review article, the biology of the development and spread of cancer and the role of PET imaging in oncology are summarized and supported by various PET images demonstrating patterns of cancer spread.

Key Words: cancer; spread; invasion; metastasis; PET

J Nucl Med Technol 2022; 50:81–89
DOI: 10.2967/jnmt.121.263534

Approximately 17 million new cancer cases were diagnosed and 10 million people died because of cancer in 2018 (*1*). The 3 most common sites of new cancers were the lung (1,368,500), prostate (1,276,100), and colorectal region (1,026,200) in men and the breast (2,088,800), colorectal region (823,300), and lung (725,400) in women in 2018 (*1*). Each year, approximately 400,000 children (0–19 y old) are diagnosed with cancer (*2*).

The development and spread of cancer is a multistep and complex process that involves a number of alterations in the cell, interactions between cancer cells and multiple cell types in the local and distant environments, and multiple molecular networks. Carcinogenesis is a multistep process with initiation, promotion, and progression phases and requires multiple mutations over a lifetime. PET/CT has been widely used for cancer imaging in the last 20 years. In this review article, the biology of cancer (development of cancer, modes and mechanisms of cancer spread) and current role of PET imaging in oncology are summarized and supported by PET images of various patterns of cancer spread.

Received Nov. 16, 2021; revision accepted Jan. 10, 2022.
For correspondence or reprints, contact Ismet Sarikaya (isarikaya99@yahoo.com).
Published online Apr. 19, 2022.

BIOLOGY OF DEVELOPMENT, INVASION, AND METASTASIS OF CANCER

Carcinogenesis is the development of cancer cells from a normal cell. In normal cells, the cell cycle is regulated by positive and negative feedback signals. The cell cycle has multiple phases, which include a quiescent or resting phase (G0), an interphase (G1, S, and G2), a mitotic phase (M), and a programmed cell death phase with checkpoints in interphase and mitosis (*3*,*4*). p53 is one of the main control proteins that suppress cell cycle progression in DNA-damaged cells and also aid DNA repair. Several genetic alterations occur in cancer cells to overcome the regulated cell growth. In most malignancies, the G1/S checkpoint is involved (*3*).

Acquired mutations are the most common cause of cancer, which can occur because of various factors such as tobacco use, radiation, viruses, chemicals, chronic inflammation, aging, and the environment. Germline mutations are the cause in about 5%–20% of malignancies (*5*). The carcinogenic process involves alteration or mutation in cancer genes, such as activation of oncogenes (e.g., HER2, RAS family, and RAF), inactivation of tumor suppressors (e.g., BRCA1, BRCA2, and p53), evasion of apoptosis genes, and defects in DNA repair genes. In up to 60% of cancers, there is mutation in the p53 gene, and in 30% of the cancers, there is mutation in the RAS/RAF/MEK/ERK pathway (*4*).

Neoplasms are derived from a single clone of cells that grow in an uncoordinated manner. The biologic characteristics and hallmarks of cancer cells include ability to generate mitogenic signals, evasion or resistance of immune killing, resistance of growth suppression, genetic instability, evasion of apoptosis, acquisition of unregulated sustained proliferation (immortality), angiogenesis, altered metabolism, inflammation, tumor heterogeneity, tissue invasion, and metastasis (*6*–*8*). Cancer cells within the tumor are morphologically, biochemically, and genetically heterogeneous. The most definite hallmark of cancer is the subset of neoplastic cells that escape through the basement membrane and penetrate the stroma (*6*).

Remodeling in cellular junctions, interaction between the cells and the extracellular matrix through cell adhesion molecules (e.g., integrins, selectins, cadherins, immunoglobulin

superfamily, and CD44), focal adhesions, and other substances (e.g., matrix metalloproteinases and EPLIN [epithelial protein lost in neoplasm]) are involved in various steps of cancer progression, cell motility, and migration (*9*). After cancer cells escape the basement membrane, tumor invades or penetrates the surrounding tissues and metastasizes to distant organs. Various promoter genes are implicated in invasion and metastasis. Detachment and escape of cells from the primary tumor mimics the developmental process known as epithelial mesenchymal transition (*9*,*10*). Degradative enzymes produced by the tumor or tumor-associated cells remodel the extracellular matrices and facilitate tumor cell invasion and progression. The tumor microenvironment consists of tumor cells and various tumor-associated host cells, which make up about half the total number of cells in malignant tumors and play a critical role in cancer initiation, progression, and metastasis (particularly cancer-associated fibroblasts expressing fibroblast activation protein-α and immune cells) (*6*,*11*). Tumor cells can disseminate as individual cells or move as collective groups (plasticity of tumor cell movement) (*12*,*13*). Tumor cells eventually migrate toward transportation compartments such as blood vessels, lymphatic channels, or celomic cavities with interconnectivity between transit compartments. Most of the distant metastases are hematogenous. Initially, the tumor receives a blood supply from the vessels in the new soil or form tubes to anastomose with the existing capillaries, but later, angiogenesis is induced for further growth of the tumor.

Growth of new blood vessels and lymphatic vessels occurs in the primary and metastatic tumor. Angiogenesis occurs via various mechanisms such as formation and outgrowth of sprouts, formation of new vasculature from existing vessels, recruitment of circulating endothelial progenitor cells, vascular mimicry, and transdifferentiation of cancer stem cells (*14*). Lymphatic enlargement and lymphangiogenesis via growth factors produced by tumor and tumor microenvironment cells occur in the primary tumor and sentinel lymph nodes (*15*).

SUMMARY OF PET IMAGING IN ONCOLOGY

PET imaging is closely related to cancer biology and pathology, because PET imaging uses various radiotracers for cancer detection based on biologic and pathologic changes in cancer cells and the tumor microenvironment. PET/CT has been widely used for cancer imaging since early 2000. PET/MRI has also become available in the last 10 years. The recent introduction of total-body PET/CT cameras allow imaging of the entire body simultaneously within a few minutes (*16*).

PET is used for initial staging, assessing response to various treatments, detecting recurrences, differentiating benign from malignant lesions, guiding biopsies, planning radiotherapy, selecting patients for treatments, searching for the primary tumor in cases with primary-unknown metastases and paraneoplastic syndromes, and predicting tumor grade, aggressiveness, heterogeneity, prognosis, and survival. There are various PET radiotracers that can detect cancer cells on the basis of increased metabolism (e.g., glucose, fatty acids, and lactate); synthesis of proteins, DNA, and cell membranes as markers of cellular proliferation; and expression of various receptors, enzymes, and tumor-associated or -specific antigens. Table 1 shows the common and uncommon PET radiotracers for cancer imaging.

^{18}F-FDG is the most commonly used PET radiotracer to image cancer. Cancer cells mainly use glucose for their energy needs (aerobic glycolysis, Warburg effect), with accelerated glucose metabolism, increased rate of glucose transport and glycolysis, overexpression of glucose transporters, and increased level of hexokinase enzyme. The tumor microenvironment also affects the glucose metabolism of cancer cells. Breast cancer, particularly invasive and inflammatory, is among the most common indications of ^{18}F-FDG PET imaging, mainly for staging (particularly stages 3 and 4), assessing response to treatments, and detecting recurrences (*17*,*18*). ^{18}F-FDG PET is indicated for initial staging of all cases of non–small cell lung cancer and initial staging of pure and combined small cell lung cancer (*17*). ^{18}F-FDG PET is used for differential diagnosis of solid solitary pulmonary nodules that are larger than 8 mm (*19*). In multiple myeloma, ^{18}F-FDG PET helps to distinguish inactive from active disease, to detect extramedullary disease, to monitor the effect of treatments, and to determine progression from smouldering myeloma. ^{18}F-FDG PET is standard for lymphoma staging (Hodgkin and various non-Hodgkin lymphomas such as diffuse large B-cell, follicular, mucosa-associated lymphoid tissue, and mantle cell subtypes) and end-of-treatment response assessment. In head and neck cancer, ^{18}F-FDG PET is indicated for detecting an occult primary tumor and is recommended for initial staging and assessing response to treatment. ^{18}F-FDG PET is recommended in anaplastic thyroid cancer and in papillary, follicular, and Hürthle cell carcinomas if stimulated thyroglobulin is more than 2–5 ng/mL and ^{131}I imaging results are negative (*17*). High-grade gliomas, particularly glioblastoma multiforme, are usually ^{18}F-FDG–avid. ^{18}F-FDG PET helps to differentiate high- from low-grade gliomas, determine the extent of tumor for treatment planning, detect recurrences, and guide biopsies. Most soft-tissue and bone sarcomas are highly ^{18}F-FDG–avid. ^{18}F-FDG PET helps in staging and assessing the response to treatment with thyrosine kinase inhibitors in gastrointestinal stromal tumors. Most paragangliomas are ^{18}F-FDG–avid, particularly cases with succinate dehydrogenase-B mutation (*20*). Malignant melanoma is highly ^{18}F-FDG–avid. ^{18}F-FDG PET is recommended for initial staging of stage 3 and 4 melanoma and can be used in earlier stages if patients have clinical signs and symptoms (*17*). ^{18}F-FDG PET can also demonstrate cancer-related complications such as tumor thrombus and emboli, fracture, and inflammatory changes.

Radiolabeled ligands of prostate-specific membrane antigen (PSMA), most notably ^{68}Ga-PSMA-11, are used for initial staging of high-risk prostate cancer and detecting recurrences with higher efficiency than ^{11}C-choline PET and ^{18}F-fluciclovine PET at low PSA levels (*21*,*22*). PSMA PET is also used

TABLE 1
Oncologic PET Radiotracers and Their Mechanisms of Uptake in Cancer

Radiotracer	Measures or targets	Uptake mechanism	Main indications studied	Availability
^{18}F-FDG	Glucose metabolism (indirect)	Is taken up via GLUT1 and phosphorylation by hexokinase	Various cancers	Widely, routine
SSTA	Somatostatin receptors	Binds mainly to subtype 2 and in lesser degree to subtypes 3 and 5	Well- and moderately differentiated NETs	Increasing
^{68}Ga-PSMA	Cellular PSMA	Binds to cellular PSMA and internalizes	Prostate cancer	Increasing
^{18}F-NaF	Osteoblastic activity	Exchanges ^{18}F ions with hydroxyl ions on surface of hydroxyapatite to form fluoroapatite	Bone metastases from various cancers	Increasing
^{18}F-FLT	Cellular proliferation (indirect)	Is phosphorylated by thymidine kinase (not incorporated into DNA)	Various cancers; NSCLC, lymphomas	Limited
^{18}F-FET	AA uptake by transporters	Enters cells by LAT1	Brain tumors, particularly gliomas	Limited
^{11}C-MET	AA uptake and protein synthesis	Enters cells by LAT1 and is involved in synthesis of proteins and phospholipids	Brain tumors, particularly gliomas	Limited
^{18}F-FLUC	AA uptake by transporters	Enter cells by AA transporter ASCT2 and LAT1	Prostate cancer	Limited
^{18}F-DOPA	^{18}F-DOPA transport, storage, and metabolism	Enters neuroendocrine cells by LAT1, is converted to dopamine by AA decarboxylase, and is trapped in vesicles via VMAT	NETs, pheo, neuroblastoma, PG, gliomas	Limited
^{11}C-choline and ^{18}F-fluorocholine	Cell membrane synthesis or cellular proliferation	Is phosphorylated by choline kinase to phosphocholine and converted to phosphatidylcholine	Prostate cancer	Limited
^{11}C-acetate	Cellular proliferation	Incorporates into cellular membrane	HCC (well-differentiated), renal cancers	Limited
^{68}Ga-FAPI	Cancer-associated fibroblasts	Binds to fibroblast activation protein on cancer-associated fibroblasts	Various cancers	Limited
^{18}F-FES	Estrogen receptor	Binds to estrogen receptor	Breast cancer, ovarian cancer	Limited
^{89}Zr-trastuzumab	Human epidermal growth factor	Binds to human epidermal growth factor	Breast cancer	Limited
^{18}F-FDHT	Androgen receptor	Binds to androgen receptor	Prostate cancer	Limited
^{124}I	Iodine metabolism	Is taken up by thyroid follicular cells via Na+/I− symporter, is oxidized by thyroid peroxidase, stays in colloid, or leaves as thyroid hormones	Well-differentiated thyroid cancer	Limited
^{124}I-MIBG	Norepinephrine transporter	Is taken up by sympathicomedullary tissue via norepinephrine transporter (uptake-1 system) and stored in neurosecretory granules	Pheo, neuroblastoma, PG	Limited
^{18}F-FMISO	Hypoxia	Nitro-group undergoes reduction in hypoxia, forms highly reactive oxygen radicals, and binds to intracellular macromolecules	Various cancers, particularly brain and HN	Limited
^{64}Cu-ATSM	Hypoxia	Accumulates in regions with higher CD133+ expression and activates hypoxia inducible factor 1 (possible mechanisms)	Various cancers, particularly brain and HN	Limited
Folate*	Folate receptor α	Binds to folate receptor-α	Various cancers	Limited
^{68}Ga-pentixafor	CXC motif chemokine receptor 4	Binds to CXC motif chemokine receptor 4	Various cancers	Limited
^{11}C-lactate	Lactate metabolism	Undergoes oxidative phosphorylation	Various cancers	Limited
Immuno-PET*	Tumor-associated antigens	Monoclonal antibodies bind to tumor-associated antigens	Various cancers	Limited

*Various radiotracers.

GLUT1 = glucose transporter 1; SSTA = ^{68}Ga-SSTAs (somatostatin analogs); NET = neuroendocrine tumor; FLT = fluorothymidine; NSCLC = non–small cell lung carcinoma; FET = fluoroethyltyrosine; AA = amino acid; LAT1 = L-type amino acid transporter; MET = methionine; FLUC = fluciclovine; ASCT2 = alanine, serine, cysteine transporter 2; ^{18}F-DOPA = 6-^{18}F-fluoro-L-dopa; VMAT = volumetric modulated arc therapy; pheo = pheochromocytoma; PG = paraganglioma; HCC = hepatocellular carcinoma; FAPI = fibroblast-activation-protein inhibitor; FES = fluoroestradiol; FDHT = fluorodihydrotestosterone; MIBG = metaiodobenzylguanidine; FMISO = fluoromisonidazole; ATSM = diacetyl-bis(N^4-methythiosemicarbazone); HN = head and neck.

for selecting patients and for assessing response to PSMA-targeted radionuclide treatments. Somatostatin receptor PET imaging has high sensitivity in detecting various well-differentiated NETs (e.g., carcinoid) expressing high somatostatin receptors (particularly subtypes 2, 3, and 5) and certain types of paragangliomas (*20*). ^{18}F-fluoroestradiol PET helps to determine the estrogen receptor status of breast and ovarian cancers. Radiolabeled amino acid tracers such as ^{11}C-methionine, 6-^{18}F-fluoro-L-dopa, and ^{18}F-fluoroethyltyrosine have high sensitivity in detecting primary and recurrent glioblastoma multiforme. ^{18}F-thymidine has been studied for grading, assessing tumor heterogeneity, and detecting recurrences in gliomas. 6-^{18}F-fluoro-L-dopa is also useful for detecting medullary thyroid carcinomas and succinate dehydrogenase-B–negative paragangliomas (*23*). Various hypoxia-imaging radiotracers help to identify tumor hypoxia, an ability that is important for radiotherapy planning, assessing tumor heterogeneity, and selecting patients for hypoxia-targeted therapeutics. Radiolabeled fibroblast activation protein inhibitors show uptake in various cancers, with promising results (*24*). Immuno-PET imaging with radiolabeled antibodies against tumor-associated or -specific antigens has been studied in detecting cancer and assessing response to treatment.

Targeted radionuclide treatment of cancer using various β- and α-particle emitters is a rapidly evolving area. By showing the presence, extent, and intensity of the target expression in the tumor, theranostic PET imaging helps in selecting patients for targeted radionuclide treatment, determining the treatment dose, and assessing response to treatment.

Precision medicine is selection of the right treatment using various diagnostic tests (molecular, imaging) and analytics for a group of individuals with certain characteristics, whereas personalized medicine is selection of the right treatment for an individual patient. PET offers various radiotracers to image tumor biomarkers such as hypoxia, angiogenesis, apoptosis, metabolism, proliferation, and antigen/receptor expression, which help to determine tumor characteristics and heterogeneity, thus helping in choosing the right treatment and in identifying resistance to therapies with early therapy-response assessment.

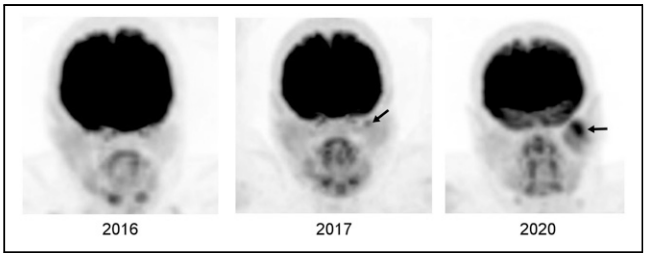

FIGURE 1. Development of parotid cancer in patient with breast cancer. Selected serial ^{18}F-FDG PET maximum-intensity-projection images of head and neck show that mild focal uptake in left parotid gland in 2017 became larger and more hypermetabolic in 2020 (arrows). Histopathologic examination showed mucoepithelial cancer. There was no abnormal uptake in left parotid gland in 2016, possibly because tumor was either absent at that time or was of microscopic or small volume below PET resolution.

^{18}F and ^{68}Ga are the most commonly used PET radionuclides for radiolabeling molecules for cancer imaging. The other PET radionuclides, such as ^{11}C and other radiometals (e.g., ^{89}Zr, ^{64}Cu, ^{86}Y, and radioisotopes of scandium and terbium) have also been studied to label various molecules. Radiometals are used mainly to label peptides, proteins, antibodies, and ligands because of their longer half-lives and longer circulation of such molecules. Longer half-life is also an advantage in shipment.

PET images are supported by various parameters to better assess radiotracer uptake and distribution in the tumor, such as SUV, metabolically active tumor volume, global metabolic tumor volume, total lesion glycolysis, dual- or multiple-time-point PET imaging with retention index, dynamic PET imaging, and parametric PET imaging with kinetic modeling and quantitative analysis (*25*). Various PET response criteria are used to better assess the response to chemotherapy, radiotherapy, and treatment with immune checkpoint inhibitors (*26*).

Figure 1 shows development of a cancer on serial PET images. Supplemental Figure 1 shows PET images of local invasion/infiltration by breast and lung cancers (supplemental materials are available at http://jnmt.snmjournals.org).

PET imaging has a well-established role in cancer management but has certain limitations such as in detecting small tumor foci and in quantifying radiotracer uptake and tumor volume and nonspecificity of radiotracers. The spatial resolution of PET has been increasing (in the range of 5–8 mm for the trunk and 3–5 mm for the brain and extremities), but smaller and microscopic or submillimetric foci cannot be detected. Ultra-high-resolution brain PET scanners are being developed that may detect brain lesions 1.6–1.8 mm in size (*27*). Current PET radiotracers are not purely cancer-specific and may show uptake in benign lesions, normal tissues, and inflammation after treatments (*28*). Low-grade and well-differentiated

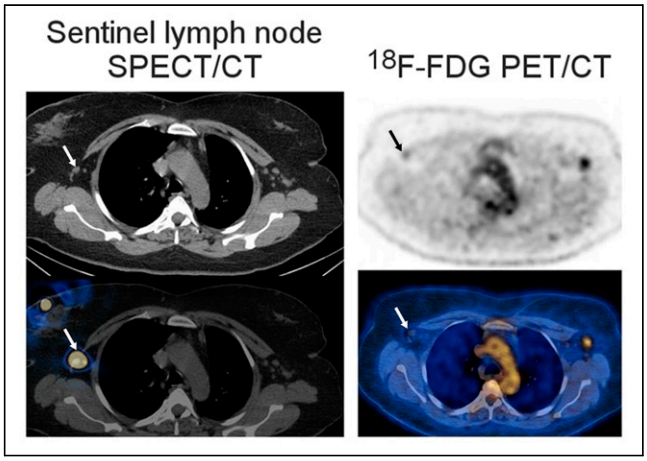

FIGURE 2. Early metastasis in sentinel lymph node as seen on transaxial SPECT/CT and ^{18}F-FDG PET/CT images of patient with newly diagnosed bilateral invasive lobular breast cancer. SPECT/CT shows right sentinel lymph node (arrows). ^{18}F-FDG PET/CT shows mild uptake in right sentinel lymph node (arrows), found on biopsy to be metastasis. ^{18}F-FDG uptake in left axillary lymph node was also due to metastasis. (Adapted from (*38*).)

tumors show low glucose metabolism, or certain tumors may use other fuels for their energy needs; the sensitivity of ^{18}F-FDG PET is reduced in such tumors. Tumor cells may lack or lose antigen or receptor expression, limiting the efficiency of PET radiotracers targeting such expression. Certain PET radiotracers that are relatively more specific for a histologic type of cancer may also show uptake in other cancer types, such as PSMA ligands. PET parameters, particularly SUV, are affected by various factors, most notably blood glucose and body mass index (*25*,*29*). SUV normalized by lean body mass or tumor-to-reference SUV ratios can be used when assessing response to treatments in obese and overweight patients (*30*,*31*). Certain medications can affect the uptake and distribution of radiotracers and should be stopped before PET studies. Calculation of local or global tumor volume with threshold- and algorithm-based methods has certain limitations, with over- or underestimation of the tumor volume (*32*). Artifacts can be seen on PET/CT images because of motion, arm positioning, and dense material or objects (*33*–*35*). Various reconstruction techniques and software are available to overcome some of these artifacts.

MODES OF METASTATIC SPREAD OF CANCER AND PET IMAGES

Metastasis Through Lymphatic System

Cancer cells enter or invade the lymphatic vessels and migrate to the tumor-draining sentinel lymph node. High interstitial fluid pressure in the tumor facilitates the entry of cancer cells into lymphatic vessels (*36*). Tumor cells and cells in the tumor microenvironment produce growth factors that promote peritumoral lymphangiogenesis, which provides tumor cells access to more lymphatic vessels. Cancer cells can also move toward and invade lymphatic vessels by sensing the chemokines produced by lymphatic endothelial cells (chemoattraction) (*36*,*37*).

Although the lymph node is filled with various immune cells, the microenvironment is immunosuppressive. Immunosuppression is believed to occur before metastasis, and the premetastatic niche emerges before cancer cells arrive (*36*). While migrating in the lymphatic vessel, tumor cells continue to grow and survive. Cancer cells can escape the tumor-draining lymph node through the efferent lymphatic vessel or invade the lymph node blood vasculature and further spread to other lymph nodes and distant organs. Figure 2 demonstrates ^{18}F-FDG uptake in a sentinel lymph node, and Supplemental Figure 2 shows uptake in lymphatic channels and lymph nodes (*38*).

Metastasis Through Vascular System

The metastatic cascade of hematogenous metastasis includes development of a metastatic cell, establishment of a premetastatic niche, motility and invasion, intravasation, dissemination and transport, cellular arrest, vascular adhesion, and extravasation and colonization (*39*).

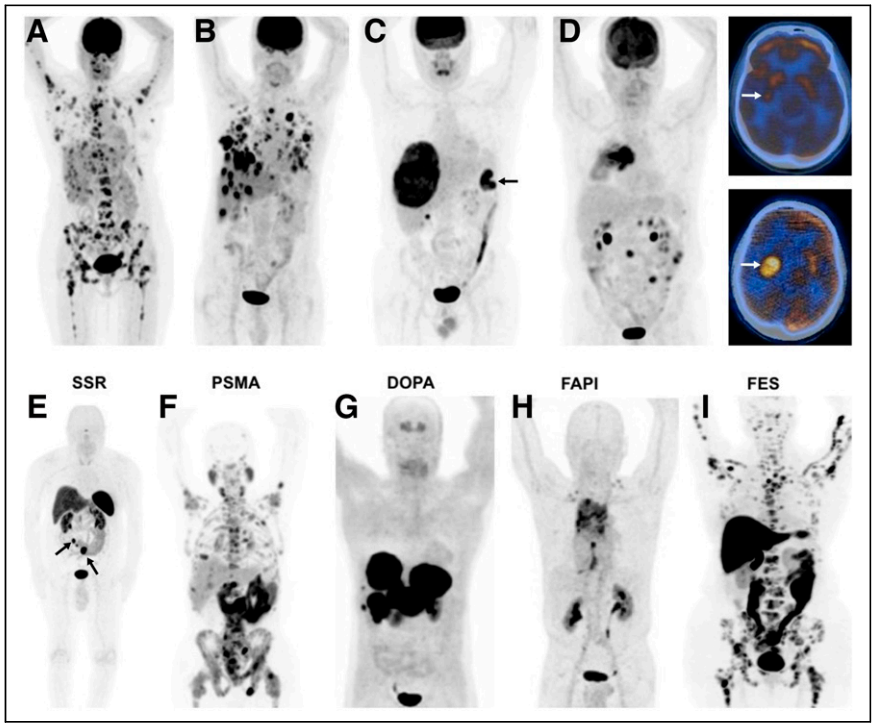

FIGURE 3. ^{18}F-FDG PET images of various cancers and metastases (A–D), and PET images with various other radiotracers (E–I). (A) Right breast cancer (invasive ductal) with multiple metastases in bones, liver, right adrenal, and right axillary lymph nodes. (B) Right breast cancer (poorly differentiated neuroendocrine tumor) with multiple metastases in lungs, liver, and right axillary lymph nodes. (C) Colon cancer in splenic flexure (arrow), with large metastasis in liver. (D) Rapid progression of brain metastasis in patient with cancer in right lung. Whole-body image (left) demonstrated hypermetabolic right lung tumor. On initial PET/CT scan, there was mild focal uptake in tail of right putamen (top right, arrow), but 3 mo later (no treatment), significant increase in size and metabolic activity of metastatic focus in brain was seen (bottom right, arrow). (E) ^{68}Ga-DOTANOC PET image of patient with small-bowel carcinoid, showing primary tumor (left arrow) and multiple mesenteric metastases (right arrow), all with high somatostatin receptor binding. (F) ^{68}Ga-PSMA-11 PET image of patient with prostate cancer, showing diffuse bone and multiple abdominal and pelvic lymph node metastases. (G) 6-^{18}F-fluoro-L-dopa PET image of patient with history of surgically treated well-differentiated ileal neuroendocrine tumor, showing intense uptake in multiple large hepatic metastases. (Adapted from (*43*).) (H) ^{68}Ga-FAPI PET image of patient with non–small cell lung carcinoma, showing intense uptake in primary tumor and metastatic foci in mediastinum and, bilaterally, in supraclavicular regions. (Adapted from (*44*).) (I)^{18}F-fluoroestradiol PET image of patient with invasive lobular breast cancer, showing extensive bone and bone marrow involvement with high estrogen receptor binding. (Adapted from (*45*).)

Before leaving the tumor, cancer cells communicate with the other parts of the body through soluble factors to establish a premetastatic niche (*40*,*41*). Stem cells are mobilized, arrive in the secondary microenvironment, and prepare it before the arrival of cancer cells. Intravasation of detached cancer cells requires partial degradation of the extracellular matrix and basement membrane underlying endothelial cells. During intravascular travel, some tumor cells evade immune attacks, but some are killed by natural killer cells or hemodynamic sheer forces (Supplemental Fig. 3) (*39*). Cancer cells evade the immune attacks by downregulating antigens and secreting substances to trick the immune system into recognizing them as normal cells or to prevent immune cells from directly killing them. By coating the cancer cells, platelets help them gain physical and immune protection. Platelets and cancer cells also secrete substances to act on the monocytes and endothelial cells. Neutrophils can protect cancer cells from natural killer cells. The efficiency of metastasis increases if the tumor cells form emboli. For extravasation, tumor cells develop adhesion to the endothelial cells and penetrate the endothelium and the basement membrane with the help of metastasis-associated macrophages in the target tissue. After extravasation, tumor foci colonize in the new soil. Cancer cells modulate and restructure the new soil. Colonized cancer cells do not always grow as soon as they seed in the new soil. They can stay dormant and become detectable in months to years. Various mechanisms are involved in cancer dormancy and reawakening.

Certain cancers seed in specific organs (organ tropism, seed-and-soil theory), a process that is regulated by multiple factors, such as interaction between tumor cells and the host microenvironment, circulation pattern, tumor-intrinsic factors, and organ-specific niches (*39*–*42*). Liver, lung, bone, and brain are the most frequent sites of distant metastases. Common sites of hematogenous metastases vary among cancer types and subtypes. Figure 3 shows PET images of distant organ metastases from various cancers (*43*–*45*).

Bone is one of the most frequent sites of tumor metastasis or spread from breast and prostate cancers and multiple myeloma. Multiple factors and expression of certain genes contribute to the homing of tumor cells to the bone. In osteolytic metastases and multiple myeloma bone lesions, the bone remodeling process is imbalanced; ephrin B2 and EphB4 expression is downregulated (*46*). There is increased osteoclastic bone resorption driven by osteoclast-activating factors produced by the tumor or cells in the bone microenvironment. Tumor cells also produce osteoblast inhibitor factors. Myeloma cells produce growth factors that stimulate the growth of bone marrow stromal cells, which in turn produce osteoclast-activating factors, such as IL-6, M-CSF, TNFa, and RANKL. In osteoblastic metastases, there is formation of new bone that is immature and of poor quality. Tumor cells secrete factors that induce osteoblastic proliferation and differentiation, such as TGF-β, VEGF, and FGF (*46*). In prostate cancer, prostate-specific antigen and other substances modify the bone microenvironment. Supplemental Figures 4–6 show the histopathology and some PET images of osteolytic and osteoblastic bone metastases (*47*).

Liver is a common site for metastases from breast, lung, and gastrointestinal malignancies. Hepatocytes interact directly with tumor cells to promote liver metastasis and promote the formation of a prometastatic niche via secretion of various substances (*42*). Hepatic stellate and Kupffer cells are also involved in inducing or facilitating liver metastasis. Lung is a common site for metastasis from breast, melanoma, and thyroid malignancies. Tumor-derived factors help tumor cell extravasation to the lung parenchyma. Neutrophils, chemokines, alveolar macrophages, and fibroblasts are involved in facilitating lung metastasis (*42*). Brain is a common metastatic site for lung cancer, breast cancer, and melanoma. Tumor cells produce certain substances to overcome the defense provided by the blood–brain barrier. Astrocytes secrete many factors, such as IL6, TGF-β, and IGF-1, to induce the growth of brain metastases (*48*). Figure 3 shows rapid progression of brain metastasis.

Metastasis Through Celomic Cavities

Peritoneal spread of the tumor can occur because of direct rupture of the tumor into the peritoneal cavity, intraperitoneal seeding from ascites, or hematogenous or lymphatic spread, depending on the type of primary tumor (*49*). Intraperitoneal seeding most commonly occurs from gastrointestinal and ovarian malignancies. During surgery or biopsy, secondary seeding may occur. Tumor cells adhere to the mesothelial lining of the peritoneum and invade the submesothelial connective tissues. Tumor cells initially grow focally in gravity-dependent recesses—in regions of stasis, pouches, paracolic gutters, the umbilicus, and subdiaphragmatic spaces—but eventually diffusely involve both the visceral and the parietal peritoneum. Peritoneal carcinomatosis

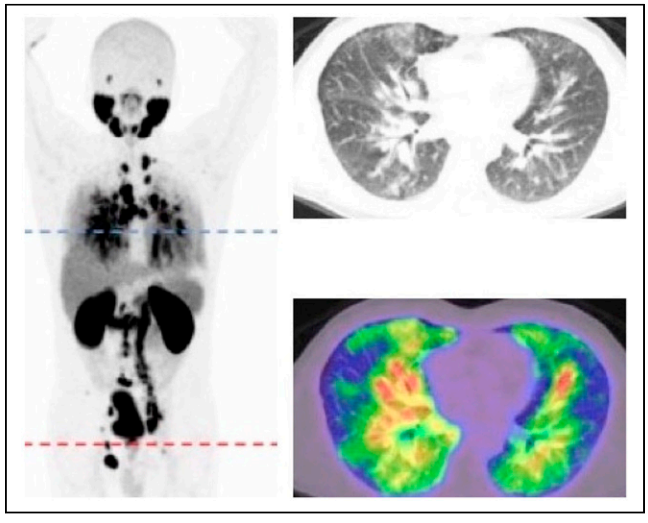

FIGURE 4. Pulmonary LC in patient with prostate cancer. Whole-body PET and transaxial CT and ^{68}Ga-PSMA ligand images show widespread thickening of interlobular septae and diffusely increased radiotracer uptake. (Adapted with permission of (*53*).)

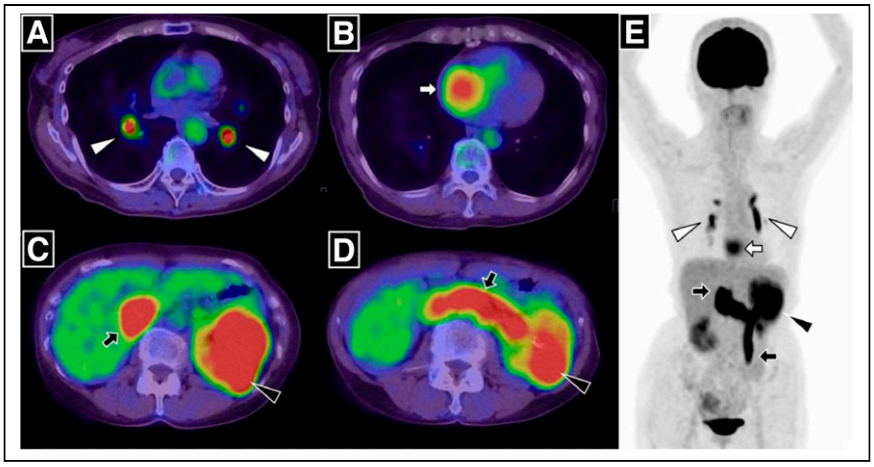

FIGURE 5. Massive pulmonary tumor emboli from intravascular tumor thrombus in patient with renal cell carcinoma. PET/CT and maximum-intensity-projection images demonstrate ^{18}F-FDG accumulation in left renal tumor, which was continuously observed in left renal vein and extended into infradiaphragmatic inferior vena cava and left ovarian vein (C, D, and E, black arrows). ^{18}F-FDG uptake in left distal pulmonary artery and right and left branches (A and E, white arrowheads) and right atrial cavity (B and E, white arrows) is also seen. (Reprinted with permission of (*55*).)

is usually associated with ascites. Supplemental Figure 7 shows ^{18}F-FDG PET/CT images of cases of peritoneal carcinomatosis.

Pleural spread of the tumor (pleural carcinomatosis) can develop as a direct extension of nearby cancer into the pleural space or through hematogenous or lymphangitic spread (*50*). Pleural tumor is usually associated with malignant pleural effusion. Pericardial spread of tumor may occur via lymphatic or hematogenous dissemination, local direct extension, or the transvenous route by various tumors.

The Krukenberg tumor is a rare metastatic signet ring cell tumor of the ovary, with primary tumor in most cases being in the stomach, colon, appendix, or breast (particularly invasive lobular carcinoma). The mechanism could be via lymphogenous, hematogenous, or transcelomic pathways (*51*).

Other Routes of Metastasis

Lymphangitic Carcinomatosis (LC). LC is diffuse infiltration and obstruction of parenchymal lymphatic channels by cancer cells, with associated inflammation. The most common location is the lungs (pulmonary LC), and rarely it can occur in other organs. Pulmonary LC is usually seen in breast, lung, stomach, pancreas, ovary, and cervix cancers. The mechanism of LC is not well understood. It may be due to retrograde tumor spread into the lymphatics through the hilar or thoracic lymph nodes as a result of obstruction in lymphatic drainage. It may also be due to antegrade movement of tumor cells from the pleura to the hilar lymph nodes through lymphatic vessels. Another possibility is hematogenous spread of metastatic disease to the lung interstitium, with subsequent lymphatic involvement. The mechanism may also be via tumor embolism (*52*). Histopathologically, cancer cells are located within or around the lymphatics in the interstitium, with edema and a desmoplastic reaction. Figure 4 shows PET/CT images of a case of pulmonary LC (*53*).

Tumor Embolism and Tumor Thrombus. Tumor embolism can occur when cancer cells from solid tumors enter the circulation as individual or clusters of cells and lodge in various sizes of arteries or due to tumor fragments from an intravascular tumor thrombus. Common sites of tumor embolism are the aortic bifurcation or the femoral, cerebral, pulmonary, renal, or splenic arteries (*54*). Within the artery, a tumor embolus may resolve, remain latent, or progress. Tumor embolism is more common in breast, lung, colon, stomach, kidney, ovary, and liver cancers. A tumor thrombus is an extension of the tumor into a vessel, mainly a vein. A tumor thrombus is most frequently associated with renal cell, adrenal cortical, and hepatocellular carcinomas and with Wilms tumor. Figure 5 shows massive tumor emboli caused by an intravascular tumor thrombus (*55*).

Tumor Spread Through Canaliculi. Tumor can spread through canaliculi such as the bile, mammary, and nasolacrimal ducts; the urinary tract; and the airways. Cancer cells

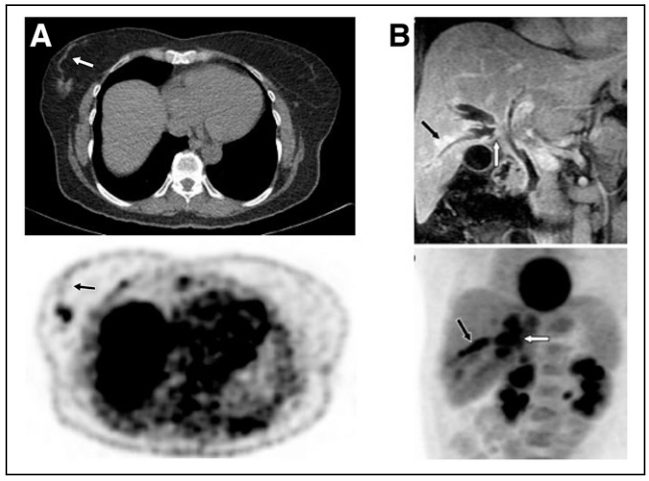

FIGURE 6. (A) Transaxial CT and ^{18}F-FDG PET images of patient with tubular breast cancer show hypermetabolic primary tumor as well as linear mild activity representing intraluminal tumor uptake either in mammary duct extending to nipple or in lymphatic channel extending to Sappey plexus (arrows). (B) Infiltrating perihilar cholangiocarcinoma with peribiliary extension. Coronal T1-weighted contrast-enhanced MR image (top) shows enhancing tumor of confluence of right ducts (white arrow), intrahepatic ductal dilation, and enhancing right peribiliary extension (black arrow), and ^{18}F-FDG PET maximum-intensity-projection image (bottom) shows ^{18}F-FDG–avid perihilar tumor (white arrow) with peribiliary extension (black arrow). (Adapted from (*56*).)

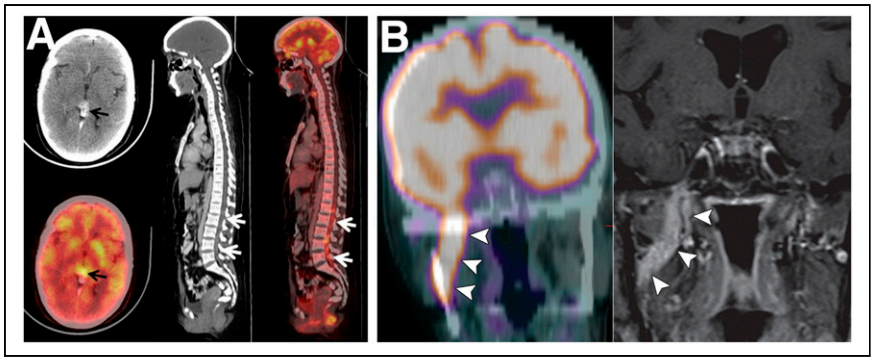

FIGURE 7. (A) Drop metastases in spinal canal from germ cell tumor of pineal gland. Head CT (top left) and ^{18}F-FDG PET (bottom left) show avidly enhancing hypermetabolic nodular lesion in pineal gland (arrows). Sagittal CT (middle) and ^{18}F-FDG PET/CT (right) show increased uptake in ill-defined densities in spinal canal extending from L1 to L5 (arrows). (Adapted from (*58*).) (B) Perineural tumor spread along V3 (mandibular) nerve. Coronal ^{18}F-FDG PET/CT (left) and contrast-enhanced T1-weighted fat-saturated MRI (right) show intense ^{18}F-FDG accumulation and abnormal enhancement along V3 (arrowheads). (Adapted with permission of (*60*).)

can also migrate along the basal side of endothelial cells without entering the lumen. Tumor spread through canaliculi or ducts can be seen as a linear area of increased uptake on PET images. Figure 6 shows PET images of tumor spread via a possible mammary duct in breast cancer and peribiliary extension of tumor in cholangiocarcinoma (*56*).

Leptomeningeal Carcinomatosis. Leptomeningeal carcinomatosis is infiltration of cancer cells in the meningeal space surrounding the brain and spinal cord, which is more commonly seen in breast cancer, lung cancer, and melanomas. Cancer cells can reach the meningeal space by hematogenous spread, direct extension or drop metastases from metastatic or primary brain tumors and then are disseminated by the cerebrospinal fluid flow in the meningeal space (*57*). Leptomeningeal carcinomatosis can also involve cranial nerves. Figure 7A shows drop metastasis into the spinal medullary cavity (*58*). Metastasis to the cerebral ventricles is rare and could be caused by intracranial or extracranial tumors.

Perineural Tumor Invasion and Perineural Tumor Spread. Perineural tumor invasion is a histopathologic (microscopic) finding of local infiltration of the nerves near the tumor, whereas perineural tumor spread is macroscopic extension of the tumor along the nerve sheath. Studies have shown that perineural tumor growth is a molecularly mediated process and that supportive cells within the peripheral nerves interact with the cancer to promote invasion and dissemination of cancer cells along the nerves (*59*). Perineural tumor growth is more commonly seen in head and neck cancers (particularly facial, mandibular, and maxillary nerves) but can also occur with various other cancers such as cancer of the pancreas, prostate, colon, or rectum. MRI is a gold standard in detecting perineural tumor spread. Figure 7B shows PET/MR images of perineural tumor spread (*60*).

CONCLUSION

The biology of the development and spread of cancer and the role of PET imaging in oncology have been summarized in this article, supported by various PET images demonstrating cancer spread patterns.

DISCLOSURE

No potential conflict of interest relevant to this article was reported.

REFERENCES

1. *Global Cancer Facts & Figures.* 4th ed. American Cancer Society; 2018:1–73.
2. Steliarova-Foucher E, Colombet M, Ries LAG, et al. International incidence of childhood cancer, 2001-10: a population-based registry study. *Lancet Oncol.* 2017;18:719–731.
3. Ok CY, Woda B, Kurian E. The pathology of cancer. In: Pieters RS, Liebmann J, eds. *Cancer Concepts: A Guidebook for the Non-Oncologist.* University of Massachusetts Medical School; 2018:1–11.
4. Malarkey DE, Hoenerhoff M, Maronpot RP. Carcinogenesis: mechanisms and manifestations. In: Haschek W, Bolon B, Ochoa R, Rousseaux C, Wallig M, eds. *Haschek and Rousseaux's Handbook of Toxicologic Pathology.* Vol 1. 3rd ed. Academic Press; 2013:107–146.
5. The genetics of cancer. Cancer.Net website. https://www.cancer.net/navigating-cancer-care/cancer-basics/genetics/genetics-cancer. Published March 2018. Accessed April 8, 2022.
6. Welch DR, Hurst DR. Defining the hallmarks of metastasis. *Cancer Res.* 2019;79:3011–3027.
7. Welch DR. Tumor heterogeneity: a 'contemporary concept' founded on historical insights and predictions. *Cancer Res.* 2016;76:4–6.
8. Hanahan D, Weinberg RA. Hallmarks of cancer: the next generation. *Cell.* 2011;144:646–674.
9. Martin TA, Ye L, Sanders AJ, Lane J, Jiang WG. Cancer invasion and metastasis: molecular and cellular perspective. NCBI website. https://www.ncbi.nlm.nih.gov/books/NBK164700/. Published 2013. Accessed April 8, 2022.
10. Tarin D. The fallacy of epithelial mesenchymal transition in neoplasia. *Cancer Res.* 2005;65:5996–6000.
11. Mareel M, Oliveira MJ, Madani I. Cancer invasion and metastasis: interacting ecosystems. *Virchows Arch.* 2009;454:599–622.
12. Wu JS, Jiang J, Chen BJ, Wang K, Tang YL, Liang XH. Plasticity of cancer cell invasion: patterns and mechanisms. *Transl Oncol.* 2021;14:100899.
13. Clark AG, Vignjevic DM. Modes of cancer cell invasion and the role of the microenvironment. *Curr Opin Cell Biol.* 2015;36:13–22.
14. Lugano R, Ramachandran M, Dimberg A. Tumor angiogenesis: causes, consequences, challenges and opportunities. *Cell Mol Life Sci.* 2020;77:1745–1770.
15. Stacker SA, Williams SP, Karnezis T, Shayan R, Fox SB, Achen MG. Lymphangiogenesis and lymphatic vessel remodelling in cancer. *Nat Rev Cancer.* 2014;14:159–172.
16. Badawi RD, Shi H, Hu P, et al. First human imaging studies with the EXPLORER total-body PET scanner. *J Nucl Med.* 2019;60:299–303.
17. NCCN practice guidelines: narrative summary of indications for FDG PET and PET/CT. amazonaws website. http://s3.amazonaws.com/rdcms-snmmi/files/production/public/images/NCCN%20Narrative%20Summary%20Feb%202016.pdf. Accessed April 26, 2022.
18. Sarikaya I. Breast cancer and PET imaging. *Nucl Med Rev Cent East Eur.* 2021;24:16–26.
19. MacMahon H, Naidich DP, Goo JM, et al. Guidelines for management of incidental pulmonary nodules detected on CT Images: from the Fleischner Society 2017. *Radiology.* 2017;284:228–243.
20. Taïeb D, Hicks RJ, Hindié E, et al. European Association of Nuclear Medicine practice guideline/Society of Nuclear Medicine and Molecular Imaging procedure standard 2019 for radionuclide imaging of phaeochromocytoma and paraganglioma. *Eur J Nucl Med Mol Imaging.* 2019;46:2112–2137.

21. Morigi JJ, Stricker PD, Leeuwen PJV, et al. Prospective comparison of ^{18}F-fluoromethylcholine versus ^{68}Ga-PSMA PET/CT in prostate cancer patients who have rising PSA after curative treatment and are being considered for targeted therapy. *J Nucl Med.* 2015;56:1185–1190.
22. Calais J, Ceci F, Eiber M, et al. ^{18}F-fluciclovine PET-CT and ^{68}Ga-PSMA-11 PET-CT in patients with early biochemical recurrence after prostatectomy: a prospective, single-centre, single-arm, comparative imaging trial. *Lancet Oncol.* 2019; 20:1286–1294.
23. Giovanella L, Treglia G, Iakovou I, Mihailovic J, Verburg FA, Luster M. EANM practice guideline for PET/CT imaging in medullary thyroid carcinoma. *Eur J Nucl Med Mol Imaging.* 2020;47:61–77.
24. Hicks RJ, Roselt PJ, Kallur KG, Tothill RW, Mileshkin L. FAPI PET/CT: will it end the hegemony of ^{18}F-FDG in oncology? *J Nucl Med.* 2021;62: 296–302.
25. Sarikaya I, Sarikaya A. Assessing PET parameters in oncologic ^{18}F-FDG studies. *J Nucl Med Technol.* 2020;48:278–282.
26. Wahl RL, Jacene H, Kasamon Y, et al. From RECIST to PERCIST: evolving considerations for PET response criteria in solid tumors. *J Nucl Med.* 2009;50(suppl 1): 122S–150S.
27. Carson R, Berg E, Badawi R, et al. Design of the NeuroEXPLORER, a next-generation ultra-high performance human brain PET imager [abstract]. *J Nucl Med.* 2021; 62(suppl 1):1120.
28. Schierz JH, Sarikaya I, Wollina U, Unger L, Sarikaya A. Immune checkpoint inhibitor related adverse effects and FDG PET/CT findings. *J Nucl Med Technol.* 2021;49:324–329.
29. Sarikaya I, Sarikaya A, Sharma P. Assessing the effect of various blood glucose levels on ^{18}F-FDG activity in the brain, liver, and blood pool. *J Nucl Med Technol.* 2019;47:313–318.
30. Zasadny KR, Wahl RL. Standardized uptake values of normal tissues at PET with 2-[fluorine 18]fluoro-2-deoxy-D-glucose: variations with body weight and a method for correction. *Radiology.* 1993;189:847–850.
31. Sarikaya I, Albatineh AN, Sarikaya A. Revisiting weight-normalized SUV and lean-body-mass-normalized SUV in PET studies. *J Nucl Med Technol.* 2020;48: 163–167.
32. Im HJ, Bradshaw T, Solaiyappan M, Cho SY. Current methods to define metabolic tumor volume in positron emission tomography: which one is better? *Nucl Med Mol Imaging.* 2018;52:5–15.
33. Sarikaya I, Sarikaya A. PET/CT image artifacts caused by the arms. *J Nucl Med Technol.* 2021;49:19–22.
34. Sarikaya I, Elgazzar AH, Sarikaya A, Alfeeli M. Normal bone and soft tissue distribution of fluorine-18-sodium fluoride and artifacts on ^{18}F-NaF PET/CT bone scan: a pictorial review. *Nucl Med Commun.* 2017;38:810–819.
35. Sarikaya I, Yeung HW, Erdi Y, Larson SM. Respiratory artefact causing malpositioning of liver dome lesion in right lower lung. *Clin Nucl Med.* 2003;28: 943–944.
36. Zhou H, Lei PJ, Padera TP. Progression of metastasis through lymphatic system. *Cells.* 2021;10:627.
37. Borsig L, Wolf MJ, Roblek M. Lorentzen, Heikenwalder H. Inflammatory chemokines and metastasis: tracing the accessory. *Oncogene.* 2014;33:3217–3224.
38. Sarikaya I, Sarikaya A. Assessing ^{18}F-FDG uptake in the sentinel lymph node in breast cancer. *J Nucl Med Technol.* 2019;47:149–153.
39. Lambert AW, Pattabiraman DR, Weinberg RA. Emerging biological principles of metastasis. *Cell.* 2017;168:670–691.
40. Psaila B, Lyden D. The metastatic niche: adapting the foreign soil. *Nat Rev Cancer.* 2009;9:285–293.
41. Kaplan RN, Rafii S, Lyden D. Preparing the "soil": the premetastatic niche. *Cancer Res.* 2006;66:11089–11093.
42. Gao Y, Bado I, Wang H, et al. Metastasis organotropism: redefining the congenial soil. *Dev Cell.* 2019;49:375–391.
43. Rust E, Hubele F, Marzano E, et al. Nuclear medicine imaging of gastro-entero-pancreatic neuroendocrine tumors: the key role of cellular differentiation and tumor grade—from theory to clinical practice. *Cancer Imaging.* 2012;12:173–184.
44. Giesel FL, Kratochwil C, Lindner T, et al. ^{68}Ga-FAPI PET/CT: biodistribution and preliminary dosimetry estimate of 2 DOTA-containing FAP-targeting agents in patients with various cancers. *J Nucl Med.* 2019;60:386–392.
45. Ulaner GA, Jhaveri K, Chandarlapaty S, et al. Head-to-head evaluation of ^{18}F-FES and ^{18}F-FDG PET/CT in metastatic invasive lobular breast cancer. *J Nucl Med.* 2021;62:326–331.
46. Roodman GD, Silbermann R. Mechanisms of osteolytic and osteoblastic skeletal lesions. *Bonekey Rep.* 2015;4:753.
47. Roudier MP, Morrissey C, True LD, et al. Histopathological assessment of prostate cancer bone osteoblastic metastases. *J Urol.* 2008;180:1154–1160.
48. Valiente M, Ahluwalia MS, Boire A, et al. The evolving landscape of brain metastasis. *Trends Cancer.* 2018;4:176–196.
49. Levy AD, Shaw JC, Sobin LH. Secondary tumors and tumorlike lesions of the peritoneal cavity: imaging features with pathologic correlation. *Radiographics.* 2009; 29:347–373.
50. Agalioti T, Giannou AD, Stathopoulos GT. Pleural involvement in lung cancer. *J Thorac Dis.* 2015;7:1021–1030.
51. Wu F, Zhao X, Mi B, et al. Clinical characteristics and prognostic analysis of Krukenberg tumor. *Mol Clin Oncol.* 2015;3:1323–1328.
52. Biswas A, Sriram PS. Getting the whole picture: lymphangitic carcinomatosis. *Am J Med.* 2015;128:837–840.
53. Tang VD, Campbell P, Pattison DA. Lymphangitic carcinomatosis from prostate cancer identified with gallium-68 prostate-specific membrane antigen positron emission tomography imaging. *Urology.* 2018;114:e1–e2.
54. Azevedo AS, Follain G, Patthabhiraman S, Harlepp S, Goetz JG. Metastasis of circulating tumor cells: favorable soil or suitable biomechanics, or both? *Cell Adh Migr.* 2015;9:345–356.
55. Ogawa Y, Abe K, Hata K, Yamamoto T, Sakai S. A case of pulmonary tumor embolism diagnosed with respiratory distress immediately after FDG-PET/CT scan. *Radiol Case Rep.* 2021;16:718–722.
56. Mar WA, Shon AM, Lu Y, et al. Imaging spectrum of cholangiocarcinoma: role in diagnosis, staging, and posttreatment evaluation. *Abdom Radiol (NY).* 2016;41: 553–567.
57. Kokkoris CP. Leptomeningeal carcinomatosis: how does cancer reach the pia-arachnoid? *Cancer.* 1983;51:154–160.
58. Jain TK, Basher RK, Sood A, Mittal BR, Prakash G, Bhatia A. ^{18}F-FDG PET/CT finding of drop metastases from germ cell tumor of pineal gland. *J Nucl Med Technol.* 2017;45:114–115.
59. Bakst RL, Glastonbury CM, Parvathaneni U, Katabi N, Hu KS, Yom SS. Perineural invasion and perineural tumor spread in head and neck cancer. *Int J Radiat Oncol Biol Phys.* 2019;103:1109–1124.
60. Paes FM, Singer AD, Checkver AN, Palmquist RA, De La Vega G, Sidani C. Perineural spread in head and neck malignancies: clinical significance and evaluation with ^{18}F-FDG PET/CT. *Radiographics.* 2013;33:1717–1736.